Ammonia Activation by Early Transition Metal Atoms (Sc, Ti, and V). Matrix Isolation Infrared Spectroscopic and Density Functional Theory Studies

Mohua Chen, Hao Lu, Jian Dong, Lei Miao, and Mingfei Zhou*

Department of Chemistry and Laser Chemistry Institute, Fudan University, Shanghai 200433, P. R. China

Received: May 7, 2002; In Final Form: September 25, 2002

Reactions of the early transition metal atoms Sc, Ti, and V with NH_3 molecules in solid argon matrix have been studied by infrared spectroscopy and density functional calculations. It is found that the ground-state metal atoms reacted with NH_3 to form the MNH_3 (M = Sc, Ti, and V) complexes spontaneously on annealing. The MNH_3 complexes underwent photochemical rearrangement to the $HMNH_2$ molecules. The $HScNH_2$ molecule further decomposed to $ScNH + H_2$ upon ultraviolet−visible irradiation. While in the $Ti + NH_3$ and $V + NH_3$ reaction systems, the novel H_2TiNH and H_2VNH species were the ultimate products generated from the photoinduced isomerization of the $HTiNH_2$ and $HVNH_2$ intermediates. All the reaction intermediates and products have been identified by isotopic substitutions and by density functional theoretical frequency calculations. Qualitative analysis of the possible reaction paths for these reactions is given, including various minima and transition states. The results have been compared with previous works covering middle transition metal atoms as well as main group atom reactions with NH_3 to obtain periodic trends for these reactions.

Introduction

The interaction of ammonia with transition metal centers is of great importance in many fields such as catalysis, surface science, and material synthesis. Ammonia is widely used as a nitrogen source in the fabrication of the transition metal nitrides.[1] Investigation of dehydrogenation of ammonia by transition metals can provide insight into the formation mechanisms of metal nitrides. The oxidative addition of N−H bond of ammonia to transition metal centers is also an important step in catalytic processes such as alkene hydroamination.[2]

Interactions of bare metal cations with ammonia and ammonia clusters have been the subject of considerable investigations.[3−16] Experimentally, it has been shown that the reactions of early transition metal cations Sc^+, Ti^+, and V^+ with ammonia lead to the formation of $ScNH^+$, $TiNH^+$, and VNH^+ as dominant products at low energies.[3−5] The production of MNH^+ has been proposed to proceed via the facile formation of a MNH_3^+ complex followed by oxidative addition to form an insertion intermediate $HMNH_2^+$.[6,8,9] In the reactions of cobalt cation, a long-lived insertion product HCo^+NH_2 has been observed.[10] The bond dissociation energies of the transition metal cation−ammonia complexes have also been determined both experimentally[13,14] and theoretically.[15,16]

The activation of the N−H bond of ammonia by the transition metal atoms as well as main group element atoms has also gained much attention. Experimentally, matrix isolation spectroscopic methods have been widely used to investigate thermal and photochemical reaction products. Interactions of alkali metals with ammonia have identified the formation of the molecular complexes.[17,18] The reactions between group 13 atoms and ammonia in solid matrixes have been studied by several groups.[19−22] The EPR study reported the formation of $Al(NH_3)_2$ and $Al(NH_3)_4$ adducts.[19] Andrews and co-workers reported that electronic excited Al atoms reacted with ammonia to form the $HAlNH_2$ and $AlNH_2$ molecules.[20] Recently, the thermal and photochemical reactions of group 13 metal M (M = Al, Ga, and In) with ammonia have been investigated by Himmel et al.; the MNH_3, $HMNH_2$, MH_2, and H_2MNH_2 species were generated and characterized.[22] It is of particular interest to know that the photochemical reactions of $HMNH_2$ (M = Al, Ga and In) are distinctly different to the ones of group 14 atoms that have been investigated recently in our laboratory.[23] On exposure to broad-band UV−visible light, the $HMNH_2$ molecules (M = Al, Ga, and In) prefer to lose one H atom to form the monovalent MNH_2 molecules, but H_2 elimination dominates the photoreaction of $HSiNH_2$ and $HGeNH_2$.

In solid matrixes, Fe, Ni, and Cu form adducts with one or two NH_3 molecules, and UV irradiation induced the insertion of the metal into an N−H bond of NH_3 with the formation of the amido derivatives $HMNH_2$ (M = Fe, Ni, and Cu), $HMNH_2NH_3$ (M = Fe or Ni), and MNH_2 (M = Cu).[24−26] The geometries, vibrational properties, energetics, and the nature of bonding of transition metal atom−ammonia complexes have also attracted several quantum chemical calculations.[27−32] The oxidative addition reactions between ammonia and the second row transition metal atoms have been theoretically investigated.[33] Geometries and energies for molecular adducts, transition states, and insertion products have been obtained, and the lowest barriers for the N−H insertion reaction were found for the early transition metal atoms with values slightly below zero.

In this paper, we present the combined matrix isolation FTIR spectroscopic and theoretical investigation on the reactions of early transition metal atoms (Sc, Ti, and V) with ammonia molecules. We will show that ground-state metal atoms react with ammonia in a solid argon matrix to form the MNH_3 complexes spontaneously on annealing. Photoisomerization to form the insertion intermediate $HMNH_2$, the imide ScNH, and the novel covalently bounded H_2MNH (M = Ti and V) molecules proceeds upon different UV−visible photolyses.

* Corresponding author. Fax: +86-21-65643532. E-mail:mfzhou@fudan.edu.cn.

10.1021/jp021130s CCC: $22.00
Published on Web 11/05/2002

Experimental and Theoretical Methods

The technique for matrix isolation infrared spectroscopic investigation has been described in detail previously.[34] The metal atoms were evaporated by the 1064 nm fundamental of a Nd: YAG laser (Spectra Physics, DCR 2, 20 Hz repetition rate, and 8 ns pulsed width) from rotating scandium, titanium, and vanadium metal targets. Typically, 5−10 mJ/pulse laser power was used. The ablated metal atoms were co-deposited with molecular NH_3 in excess argon onto a 11 K CsI window at a rate of 2−4 mmol/h. The CsI window was mounted on a copper holder at the cold end of the cryostat (Air Products Displex DE 202) and maintained by a closed-cycle helium refrigerator (Air Products Displex 1R02W). FTIR spectra were recorded by a Bruker IFS 113v Fourier transform infrared spectrometer equipped with a DTGS detector with a resolution of 0.5 cm^{-1}. Isotopic $^{15}NH_3$ was prepared by thermal dissociation of $(^{15}NH_4)_2SO_4$ (98%). Mixed $NH_3 + NH_2D + NHD_2 + ND_3$ was obtained by thermal dissociation of partially deuterated $(NH_3)_2SO_4$ prepared through exchange by D_2O. Matrix samples were annealed at different temperatures and subjected to different wavelength photolyses using a high-pressure mercury lamp (250W, without globe) and glass filters.

Density functional calculations were performed using the Gaussian 98 program.[35] The three-parameter hybrid functional according to Becke with additional correlation corrections due to Lee, Yang, and Parr were used (B3LYP).[36,37] Recent calculations have shown that this hybrid functional can provide accurate results for the geometries and vibrational frequencies for transition metal containing compounds.[38] The 6-311++G-(d,p) basis sets were used for H and N atoms, the all electron basis set of Wachters−Hay as modified by Gaussian was used for metal atoms.[39,40] Reactants, various possible transition states, intermediates, and products were fully optimized. The vibrational frequencies were calculated with analytic second derivatives, and zero point vibrational energies (ZPVE) were derived. Transition-state optimizations were done with the synchronous transit-guided quasi-Newton (STQN) method,[41] followed by the vibrational frequency calculations showing the obtained structures to be true saddle points.

Results and Discussions

The IR spectra will be presented, and the product absorptions will be assigned by consideration of the frequencies and isotopic shifts of the observed bands and by comparisons with DFT frequency calculations. We will then focus on the reaction mechanisms and the potential energy surfaces of the corresponding M + NH_3 reactions (M denotes Sc, Ti, and V).

Infrared Spectra. Experiments were done with different ammonia concentrations ranging from 0.1% to 0.5% in argon. Representative infrared spectra for the reactions of laser-ablated Sc, Ti, and V atoms with ammonia in excess argon in selected regions are shown in Figures 1−3, respectively, and the product absorptions are listed in Tables 1−3. The stepwise annealing and photolysis behavior of the product absorptions is also shown in the figures and will be discussed below. Nitrogen-15 and deuterium substitution experiments were employed for product identification through isotopic shift and splitting, and the isotopic counterparts are also listed in Tables 1−3. Typical spectra using $^{14}NH_3 + {}^{15}NH_3$ and $NH_3 + NH_2D + NHD_2 + ND_3$ samples in selected regions are shown in Figures 4−7, respectively.

Calculation Results. DFT/B3LYP/6-311++G(d,p) calculations were performed on three MNH_3 isomers, namely, the MNH_3 complexes, the inserted $HMNH_2$ molecules, and the H_2MNH molecules. The optimized geometric parameters are shown in Figure 8, and the vibrational frequencies and intensities are listed in Tables 4−6, respectively. All three MNH_3 complexes were predicted to have C_{3v} symmetry and are stable with respect to ground-state metals and NH_3. The inserted $HMNH_2$ molecules were calculated to be planar and are the most stable isomers on the potential energy surfaces. No

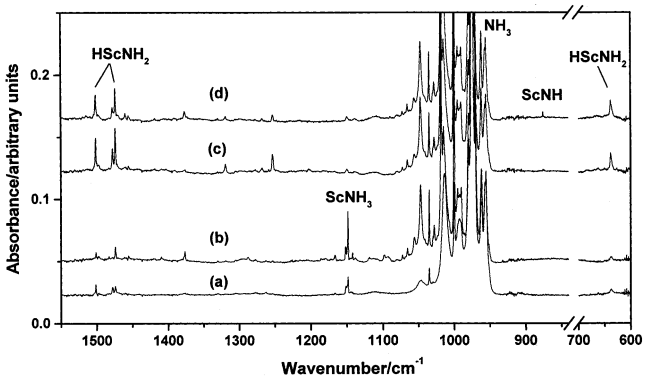

Figure 1. Infrared spectra in the 1550−600 cm^{-1} region from co-deposition of laser-ablated Sc atoms with 0.2% NH_3 in argon: (a) 1 h sample deposition at 11 K; (b) after 25 K annealing; (c) after 20 min $\lambda > 290$ nm photolysis; (d) after 20 min full arc photolysis.

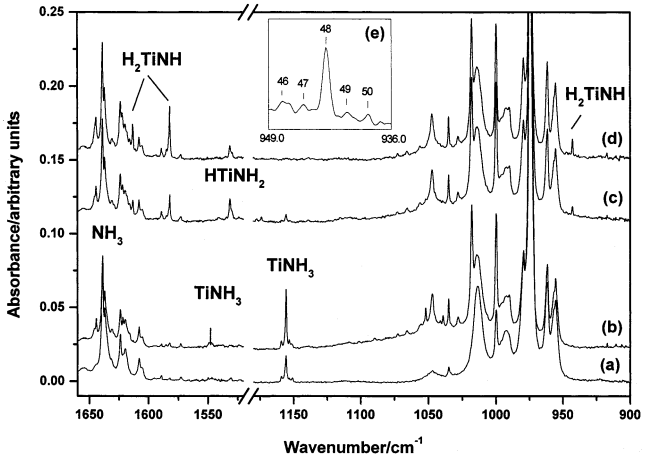

Figure 2. Infrared spectra in the 1660−1520 and 1180−900 cm^{-1} regions from co-deposition of laser-ablated Ti atoms with 0.2% NH_3 in argon: (a) 1 h sample deposition at 11 K; (b) after 25 K annealing; (c) after 20 min $\lambda > 400$ nm photolysis; (d) after 20 min $\lambda > 290$ nm photolysis; (e) the absorptions of sample (d) in the 949.0−936.0 cm^{-1} region. The labeled numbers corresponds to the ^{46}Ti, ^{47}Ti, ^{48}Ti, ^{49}Ti, and ^{50}Ti isotopomers of H_2TiNH, respectively.

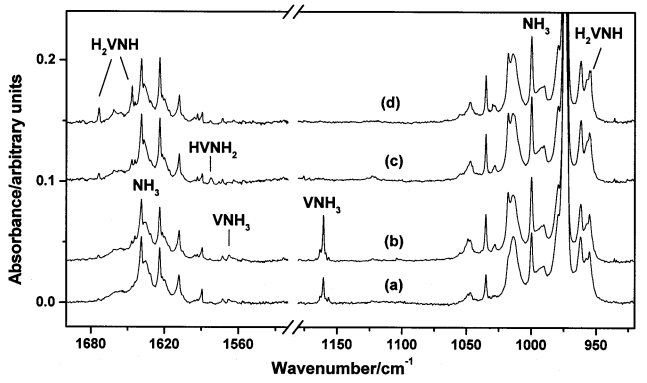

Figure 3. Infrared spectra in the 1700−1520 and 1180−920 cm^{-1} regions from co-deposition of laser-ablated V atoms with 0.2% NH_3 in argon: (a) 1 h sample deposition at 11 K; (b) after 25 K annealing; (c) after 20 min $\lambda > 400$ nm photolysis; (d) after 20 min $\lambda > 290$ nm photolysis.

TABLE 1: Infrared Absorptions (cm^{-1}) from Co-deposition of Laser-Ablated Sc Atoms with Ammonia in Excess Argon

NH_3	$^{15}NH_3$	ND_3	assignment	
1501.3	1496.7	1121.9	$HScNH_2$	NH_2 scissoring
1474.0	1473.6	1063.4	$HScNH_2$	ν(Sc−H)
1376.3	1376.3	992.9	$(HSc)_2NH$	ν_{asy}(Sc−H)
1319.3	1319.3		(H_2ScX)	$\nu_{sym}(ScH_2)$
1253.0	1253.0		(H_2ScX)	$\nu_{asy}(ScH_2)$
1148.3	1142.1	891.0	$ScNH_3$	$\delta_{sym}(NH_3)$
875.9	855.8		ScNH	ν(Sc−NH)
638.1	626.7	601.9	$HScNH_2$	ν(Sc−NH_2)

TABLE 2: Infrared Absorptions (cm^{-1}) from Co-deposition of Laser-Ablated Ti Atoms with Ammonia in Excess Argon

$^{14}NH_3$	$^{15}NH_3$	ND_3	assignment	
1613.1	1613.0	1160.1	H_2TiNH	$\nu_{sym}(TiH_2)$
1582.1	1582.1	1148.5	H_2TiNH	$\nu_{asy}(TiH_2)$
1547.7	1542.7		$TiNH_3$	$\delta_{asy}(NH_3)$
1531.7	1531.5	1104.2	$HTiNH_2$	ν(Ti−H)
1155.6	1149.0		$TiNH_3$	$\delta_{sym}(NH_3)$
947.6			$H_2{}^{46}TiNH$	
945.3			$H_2{}^{47}TiNH$	
942.9	922.3	919.7	$H_2{}^{48}TiNH$	ν(Ti−NH)
940.7			$H_2{}^{49}TiNH$	
938.3			$H_2{}^{50}TiNH$	

TABLE 3: Infrared Absorptions (cm^{-1}) from Co-deposition of Laser-Ablated V Atoms with Ammonia in Excess Argon

NH_3	$^{15}NH_3$	ND_3	assignment	
1673.7	1673.7	1207.2	H_2VNH	$\nu_{sym}(VH_2)$
1646.8	1646.8	1193.5	H_2VNH	$\nu_{asy}(VH_2)$
1582.3	1582.3	1143.2	$HVNH_2$	ν(V−H)
1567.2	1562.9		VNH_3	$\delta_{asy}(NH_3)$
1160.5	1154.2		VNH_3	$\delta_{sym}(NH_3)$
954.3	932.8		H_2VNH	ν(V−NH)

minimum was found for H_2ScNH. Geometry optimization on doublet H_2ScNH converged to ScNH + H_2. However, stable structures were optimized for H_2TiNH and H_2VNH.

Similar calculations were also done on metal imides MNH. The optimized structures are shown in Figure 8, and the vibrational frequencies and intensities are listed in Table 7.

Assignments

MNH_3. The 1148.3 cm^{-1} band in the Sc + NH_3 experiments appeared after sample deposition and markedly increased on sample annealing to 25 K. This band was destroyed on mercury lamp photolysis with a 290 nm long-wavelength pass filter. It shifted to 1142.1 and 891.0 cm^{-1}, respectively, in $^{15}NH_3$ and ND_3 experiments and gave an isotopic $^{14}N/^{15}N$ ratio of 1.0054 and H/D ratio of 1.2888. These isotopic ratios are close to the corresponding ratios ($^{14}N/^{15}N$ 1.0043 and H/D 1.2820) of the ν_2 mode of the NH_3 monomer in an argon matrix.[42] In the mixed $^{14}NH_3$ + $^{15}NH_3$ spectra, doublet isotopic structure was observed, which confirms that only one NH_3 unit is involved in this mode. Following the examples of MNH_3 (M = Al, Fe, Ni, Cu, etc.) complexes that have been previously reported,[20,22,24−26] the 1148.3 cm^{-1} band is assigned to the symmetric NH_3-bending vibration of the $ScNH_3$ complex. DFT calculation predicted that the $ScNH_3$ complex has a ^2E ground state, with a symmetric NH_3-bending vibration of 1186.9 cm^{-1}. The calculated $^{14}N/^{15}N$ and H/D ratios of 1.0058 and 1.3030 are very close to the experimental values, as listed in Table 8.

A similar band at 1155.6 cm^{-1} in the Ti + NH_3 reaction is assigned to the symmetric NH_3 bending vibration of the $TiNH_3$ complex. This band was weak after sample deposition at 11 K but was greatly increased on low-temperature annealing and was

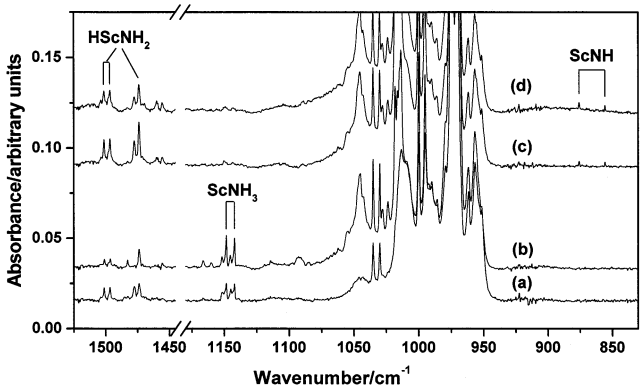

Figure 4. Infrared spectra in the 1525−1445 and 1180−820 cm^{-1} regions from co-deposition of laser-ablated Sc atoms with 0.1% $^{14}NH_3$ + 0.1% $^{15}NH_3$ in argon: (a) 1 h sample deposition at 11 K; (b) after 25 K annealing; (c) after 20 min λ > 290 nm photolysis; (d) after 20 min full arc photolysis.

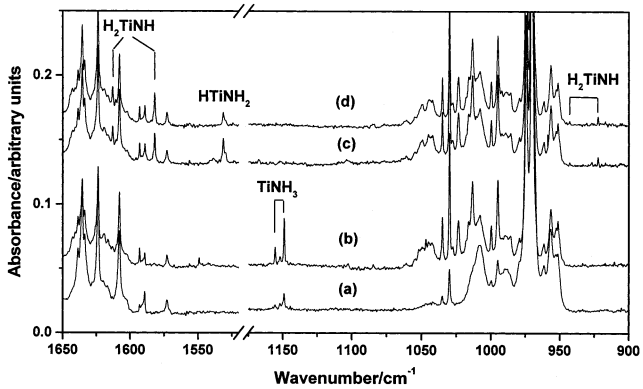

Figure 5. Infrared spectra in the 1650−1520 and 1175−900 cm^{-1} regions from co-deposition of laser-ablated Ti atoms with 0.05% $^{14}NH_3$ + 0.15% $^{15}NH_3$ in argon: (a) 1 h sample deposition at 11 K; (b) after 25 K annealing; (c) after 20 min λ > 400 nm photolysis; (d) after 20 min λ > 290 nm photolysis.

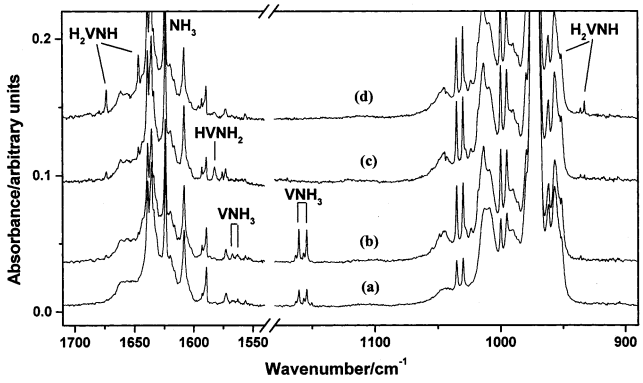

Figure 6. Infrared spectra in the 1710−1540 and 1180−890 cm^{-1} regions from co-deposition of laser-ablated V atoms with 0.1% $^{14}NH_3$ + 0.1% $^{15}NH_3$ in argon: (a) 1 h sample deposition at 11 K; (b) after 25 K annealing; (c) after 20 min λ > 400 nm photolysis; (d) after 20 min λ > 290 nm photolysis.

essentially eliminated on mercury lamp photolysis with a 400 nm long-wavelength pass filter. The $Ti^{15}NH_3$ counterpart was observed at 1149.0 cm^{-1}. The $TiND_3$ counterpart could not be observed due to band overlap, but the $TiNH_2D$ and $TiNHD_2$ absorptions were clearly observed at 1073.7 and 990.4 cm^{-1} in the NH_3 + NH_2D + NHD_2 + ND_3 experiments. A very weak band at 1547.7 cm^{-1} exhibited the same annealing and photolysis behavior as the 1155.6 cm^{-1} band and is assigned to the antisymmetric NH_3 bending mode of $TiNH_3$. The antisymmetric

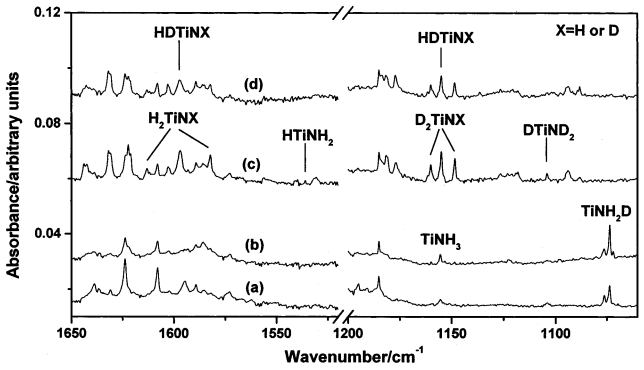

Figure 7. Infrared spectra in the 1650−1490 and 1200−1040 cm^{-1} regions from co-deposition of laser-ablated Ti atoms with 0.025% NH_3 + 0.075% NH_2D + 0.075% NHD_2 + 0.025% ND_3 in argon: (a) 1 h sample deposition at 11 K; (b) after 25 K annealing; (c) after 20 min $\lambda > 290$ nm photolysis; (d) after 20 min full arc photolysis.

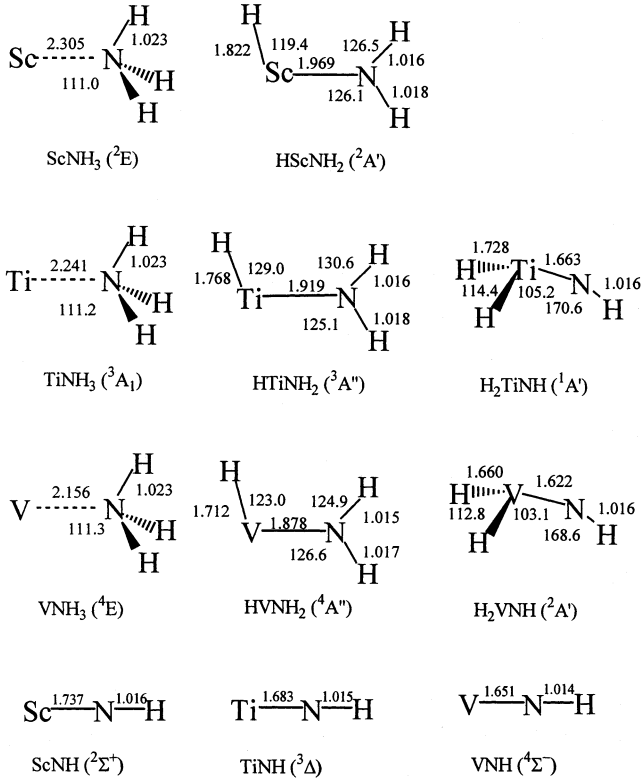

Figure 8. Calculated geometric parameters (bond length in angstrom, bond angle in degree) for the MNH_3 isomers and the MNH molecules.

TABLE 4: Calculated Vibrational Frequencies (cm^{-1}) and Intensities (km/mol) of the Ground-State MNH_3 Complexes

mode	symmetry	$ScNH_3$ (^{2}E)	$TiNH_3$($^3A_1$)	VNH_3(^{4}E)
ν_{asy}(N−H)	e	3473.1(30)	3486.0(32)	3482.1(31)
ν_{sym}(N−H)	a_1	3350.3(243)	3365.3(173)	3363.6(160)
δ_{asy}(NH_3)	e	1618.9(34)	1628.0(28)	1629.8(28)
δ_{sym}(NH_3)	a_1	1186.9(227)	1193.1(210)	1204.4(197)
ρ(NH_3)	e	397.7(52)	450.8(29)	485.8(23)
ν(M−N)	a_1	310.5(14)	331.0(8)	354.5(9)

bending vibration of $Ti^{15}NH_3$ was observed at 1542.7 cm^{-1}. DFT calculations predicted a $^3A_1$ ground-state $TiNH_3$ with strong symmetric NH_3 bending vibration at 1193.1 cm^{-1} and weak antisymmetric NH_3 bending vibration at 1628.0 cm^{-1}, respectively, in good agreement with experimental observations.

A weak absorption at 1567.2 cm^{-1} and a strong absorption at 1160.5 cm^{-1} in the V + NH_3 reaction are assigned to the VNH_3 complex. Analogous to the $ScNH_3$ and $TiNH_3$ absorptions, these two bands markedly increased upon annealing and were destroyed on $\lambda > 400$ nm photolysis and showed essentially NH_3 bending vibrational isotopic ratios (Table 8). The doublet absorptions in the mixed $^{14}NH_3$ + $^{15}NH_3$ isotopic experiments verify the participation of one NH_3 unit in this molecule. The DFT calculations predicted for VNH_3 has a ^{4}E ground state, with symmetric and antisymmetric NH_3 bending vibrations at 1204.4 and 1629.8 cm^{-1}, and isotopic frequency ratios in very good agreement with experiment, as listed in Table 8.

For all three MNH_3 complexes, the N−H stretching vibrations were not observed due to weakness. Similar to previous

TABLE 5: Calculated Vibrational Frequencies (cm^{-1}) and Intensities (km/mol) of the Ground-State $HMNH_2$ Molecules

mode	symmetry	$HScNH_2$ (^{2}A′)	$HTiNH_2$ (^{3}A″)	$HVNH_2$ (^{4}A″)
ν_{sym}(N−H)	a′	3576.5(15)	3584.6(22)	3588.9(18)
ν_{asy}(N−H)	a′	3492.2(31)	3488.4(22)	3499.3(18)
ν(M−H)	a′	1531.3(270)	1575.9(442)	1625.4(379)
NH_2 scissoring	a′	1540.7(236)	1540.8(45)	1542.3(29)
ν(M−NH_2)	a′	637.3(174)	664.7(188)	665.8(176)
NH_2 out-of-plane rock	a″	499.6(133)	509.7(191)	511.9(215)
NH_2 wagging	a′	472.0(38)	493.4(34)	531.2(57)
MH in-plane def	a′	287.9(44)	337.2(53)	350.0(93)
MH out-of-plane def	a″	152.4(56)	315.0(3)	302.9(22)

TABLE 6: Calculated Vibrational Frequencies (cm^{-1}) and Intensities (km/mol) of the Ground-State H_2MNH Molecules

mode	symmetry	H_2TiNH	H_2VNH
ν(N−H)	a′	3578.1(109)	3581.7(129)
ν_{sym}(MH_2)	a′	1700.4(257)	1776.6(212)
ν_{asy}(MH_2)	a″	1664.7(496)	1751.9(405)
ν(M−NH)	a′	1023.5(204)	1040.6(140)
δ(MH_2)	a′	630.1(84)	646.7(75)
δ(N−H)	a′	555.3(280)	544.8(265)
twist	a”	503.8(10)	532.8(6)
MH_2 out-of-plane def	a′	430.3(158)	435.3(72)
MH_2 in plane def	a″	393.5(137)	410.4(155)

TABLE 7: Calculated Vibrational Frequencies (cm^{-1}) and Intensities (km/mol) of the Ground-State MNH Molecules

mode	symmetry	ScNH ($^2\Sigma^+$)	TiNH ($^3\Delta$)	VNH ($^4\Sigma^-$)
ν(N−H)	σ	3557.5(47)	3579.2(76)	3582.7(62)
ν(M−NH)	π	944.5(89)	978.1(92)	953.9(123)
MNH bending	π	527.8(182)	478.1(214)	446.9(278)

TABLE 8: Comparison of the Observed and Calculated Isotopic Frequency Ratios of the Reaction Products

		$^{14}N/^{15}N$		H/D	
molecule	mode	obsd	calcd	obsd	calcd
$ScNH_3$	δ_{sym}(NH_3)	1.0054	1.0058	1.2888	1.3030
$TiNH_3$	δ_{asy}(NH_3)	1.0032	1.0018		1.3805
	δ_{sym}(NH_3)	1.0057	1.0057		1.3058
VNH_3	δ_{asy}(NH_3)	1.0028	1.0017		1.3806
	δ_{sym}(NH_3)	1.0055	1.0046		1.3046
$HScNH_2$	NH_2 scissoring	1.0031	1.0019	1.3382	1.3452
	ν(Sc−H)	1.0003	1.0014	1.3861	1.3962
	ν(Sc−NH_2)	1.0182	1.0205	1.0601	1.0632
$HTiNH_2$	ν(Ti−H)	1.0001	1.0000	1.3872	1.3983
$HVNH_2$	ν(V−H)	1.0000	1.0000	1.3841	1.3985
H_2TiNH	ν_{sym}(TiH_2)	1.0001	1.0001	1.3905	1.4039
	ν_{asy}(TiH_2)	1.0000	1.0000	1.3775	1.3891
	ν(Ti−NH)	1.0223	1.0231	1.0252	1.0340
H_2VNH	ν_{sym}(VH_2)	1.0000	1.0000	1.3864	1.4038
	ν_{asy}(VH_2)	1.0000	1.0001	1.3798	1.3912
	ν(V−NH)	1.0233	1.0234		1.0344
ScNH	ν(Sc−NH)	1.0235	1.0240		1.0292

theoretical calculations,[28] the symmetric N−H stretching vibrations were predicted to be remarkably enhanced on complexation. It seems that DFT calculations overestimated the intensities of the N−H stretching vibrations of these complexes.

$HMNH_2$. Three absorptions at 1501.3, 1474.0, and 638.1 cm^{-1} in the Sc + NH_3 experiments were tracked throughout all the experiments, suggesting that they are due to different vibrational modes of the same molecule. These three bands are assigned to the $HScNH_2$ molecule on the basis of isotopic substitutions as well as DFT calculations. These three bands are weak on sample deposition, slightly decreased on 25 K annealing, and greatly increased on $\lambda > 290$ nm broadband photolysis at the expense of the $ScNH_3$ absorption. These three bands were the dominant absorptions after photolysis. The 1474.0 cm^{-1} band showed a very small nitrogen-15 shift but was shifted to 1063.4 cm^{-1} with ND_3 and gave an isotopic H/D ratio of 1.3861. The band position, as well as the isotopic H/D ratio, is close to the Sc−H stretching vibration of the HScOH molecule (1482.6 cm^{-1}, H/D ratio 1.3876 in solid argon),[43,44] which suggests that this band is due to a Sc−H stretching vibration. The 1501.3 cm^{-1} band shifted to 1496.7 cm^{-1} with $^{15}NH_3$ and to 1121.9 cm^{-1} with ND_3 and gave an isotopic $^{14}N/^{15}N$ ratio of 1.0031 and a H/D ratio of 1.3382, respectively. The 638.1 cm^{-1} band went to 626.7 cm^{-1} in $^{15}NH_3$ and to 601.9 cm^{-1} with ND_3 and exhibited an isotopic $^{14}N/^{15}N$ ratio of 1.0182 and a H/D ratio of 1.0601. The band positions and isotopic frequency ratios are appropriate for NH_2 scissoring and Sc−NH_2 stretching vibrations of an amido unit. Similar molecules such as $HAlNH_2$, $HFeNH_2$, and $HNiNH_2$ have also been observed in previous matrix isolation studies. [20,22,24−26]

Density functional calculations were done to get the equilibrium geometry of the proposed $HScNH_2$ molecule. The results are shown in Figure 8. The $^2A'$ ground-state $HScNH_2$ is planar with the two N−H bonds slightly nonequivalent. The calculated frequencies provide excellent support for the identification of this molecule. As listed in Tables 5 and 8, the Sc−H stretching, NH_2 scissoring, and Sc−NH_2 stretching vibrational modes were calculated at 1531.3, 1540.7, and 637.3 cm^{-1}, respectively, with the isotopic ratios in very good agreement with experiment.

The band at 1531.7 cm^{-1} in the Ti + NH_3 reaction appeared only after $\lambda > 400$ nm photolysis when the $TiNH_3$ absorptions were disappeared. Subsequent mercury lamp photolysis with a 290 nm long-wavelength pass filter markedly decreased the 1531.7 cm^{-1} band with coincident increase of the 1613.1, 1582.1, and 942.9 cm^{-1} bands, which will be assigned to the H_2TiNH molecule. The 1531.7 cm^{-1} band exhibited a very small nitrogen-15 shift but a large deuterium shift (shifted to 1104.2 cm^{-1}). The isotopic H/D ratio of 1.3872 indicates that this band is due to a Ti−H stretching vibration. The 1531.7 cm^{-1} band is assigned to the Ti−H stretching vibration of the $HTiNH_2$ molecule. For comparison, we note that the Ti−H stretching mode of the HTiOH molecule was reported at 1549.1 cm^{-1} in solid argon.[45] On the basis of our DFT calculation, the $HTiNH_2$ molecule has a $^3A''$ ground state with planar structure analogous to $HScNH_2$. The Ti−H stretching vibration was predicted at 1575.9 cm^{-1} and is the most intense mode for this molecule.

The weak band at 1582.3 cm^{-1} in the V + NH_3 reaction is tentatively assigned to the V−H stretching vibration of the $HVNH_2$ molecule. As shown in Figure 3, the 1582.3 cm^{-1} band appeared only after $\lambda > 400$ nm photolysis when the VNH_3 absorptions were wiped out. It was almost destroyed on $\lambda > 290$ nm photolysis whereas the absorptions at 1673.7, 1646.8, and 954.3 cm^{-1} were produced. The most intense V−H stretching mode for the $^4A''$ ground-state $HVNH_2$ was calculated at 1625.4 cm^{-1}.

For $HTiNH_2$ and $HVNH_2$, only the most intense metal−H stretching vibrational mode was experimentally observed. As listed in Table 5, the NH_2 scissoring vibration of $HTiNH_2$ and $HVNH_2$ was predicted to have a much lower intensity than the metal-H stretching mode and could not be observed in our experiment. However, the metal−NH_2 stretching and NH_2 out-of-plane rocking vibrations were predicted to have appreciable intensities. We were not able to observe these bands. We note that the signal-to-noise ratio in the low-frequency region is low. Another possibility is that DFT calculations overestimated the intensities of these vibrational modes.

H_2MNH (M = Ti, V). Absorptions at 1613.1, 1582.1, and 942.9 cm^{-1} appeared together upon photolysis. The 942.9 cm^{-1} band shifted to 922.3 cm^{-1} with $^{15}NH_3$ and to 919.7 cm^{-1} with ND_3. The isotopic $^{14}N/^{15}N$ and H/D ratios were 1.0223 and 1.0252, respectively, suggesting a Ti−NH stretching vibration. In the mixed $^{14}NH_3$ + $^{15}NH_3$ experiment, only pure isotopic counterparts were observed and confirmed that only one NH is involved in this mode. The natural abundance titanium isotopic splittings of the 942.9 cm^{-1} band can be clearly resolved at 947.6, 945.3, 940.7, and 938.3 cm^{-1}, corresponding to the ^{46}Ti, ^{47}Ti, ^{49}Ti, and ^{50}Ti isotopomers, respectively,[46] as shown in Figure 2e. The similar titanium isotopic splittings were also observed for the Ti−O stretching mode of H_2TiO.[45] Although it is difficult to give a quantitative comparison of the relative intensities of these absorptions due to weakness, the band contour suggests the participation of only one titanium atom. The 1613.1 and 1582.1 cm^{-1} bands showed no obvious nitrogen-15 shift but were shifted to 1160.1 and 1148.5 cm^{-1} in deuterium-substituted experiments. The H/D ratios of 1.3905 and 1.3775 are characteristic of Ti−H stretching vibrations. In the mixed NH_3 + NH_2D + NHD_2 + ND_3 experiments, two additional bands at 1597.4 and 1155.0 cm^{-1} were observed, suggesting that two equivalent hydrogen atoms were involved in these two modes. Accordingly, we assign the 1613.1, 1582.1, and 942.9 cm^{-1} bands to the symmetric and antisymmetric TiH_2 stretching and Ti−NH stretching vibrations of the H_2TiNH molecule. The 1597.4 and 1155.0 cm^{-1} bands observed in the NH_3 + NH_2D + NHD_2 + ND_3 experiment are due to Ti−H and Ti−D stretching vibrations of the HDTiNH or HDTiND molecules. Similar TiH_2 stretching vibrations have been observed at 1646.8 and 1611.9 cm^{-1} for the H_2TiO molecule in solid argon.[45]

The H_2TiNH assignment receives further support from DFT calculations. As shown in Figure 8, the H_2TiNH molecule was predicted to have a $^1A'$ ground state with nonplanar structure. The symmetric and antisymmetric TiH_2 stretching and the Ti−NH stretching vibrations were calculated at 1700.4, 1664.7, and 1023.5 cm^{-1}, respectively, which require scale factors of 0.949, 0.950, and 0.921 to fit the experimental values. As also listed in Table 8, the calculated isotopic ratios also add strong support on the H_2TiNH assignment. Besides the H/D and $^{14}N/^{15}N$ ratios, the calculated titanium isotopic ratios of the Ti−NH stretching mode (1.0055 for $^{46}Ti/^{48}Ti$, 1.0027 for $^{47}Ti/^{48}Ti$, and 0.9974 for $^{49}Ti/^{48}Ti$) were also in good agreement with the experimental values of 1.0050, 1.0026, and 0.9977, respectively.

Similar bands at 1673.7, 1646.8, and 954.3 cm^{-1} in the V + NH_3 reaction are assigned to the symmetric and antisymmetric VH_2 stretching and V−NH stretching vibrations of the H_2VNH molecule following the example of H_2TiNH. DFT calculations predicted that the H_2VNH molecule has a $^2A'$ ground state with

nonplanar structure, with the three above-mentioned vibrational modes at 1776.6, 1751.9n and 1040.6 cm^{-1}, respectively.

ScNH. In the Sc + NH_3 experiments, a band at 875.9 cm^{-1} appeared only on full arc photolysis ($\lambda > 250$ nm) when the $HScNH_2$ absorptions decreased. It shifted to 855.8 cm^{-1} with $^{15}NH_3$ and exhibited an isotopic $^{14}N/^{15}N$ ratio of 1.0235, indicative of a Sc−NH stretching vibration. In the mixed $^{14}NH_3 + {}^{15}NH_3$ spectra, a doublet at 875.9 and 855.8 cm^{-1} was observed, which confirmed that only one NH is involved in this mode. The 875.9 cm^{-1} band is assigned to the ScNH molecule. Our DFT calculations predicted that the ScNH molecule has a $^2\Sigma^+$ ground state with linear structure. As listed in Table 7, the Sc−NH stretching vibration was calculated at 944.5 cm^{-1}, with an isotopic $^{14}N/^{15}N$ ratio of 1.0240, which matches the experimental values extremely well. The N−H stretching and bending modes were calculated to have comparable intensities with the Sc−NH mode, but these two modes were not observed in our IR spectra due to high noise level at these frequency regions.

The ScNH molecule has been produced in the reaction of laser-ablated scandium with ammonia in the gas phase and detected by laser induced fluorescence spectroscopy.[47] The harmonic Sc−NH stretching vibration was estimated at 896 cm^{-1}, in good agreement with our matrix value.

Other Absorptions. In the Sc + NH_3 reaction, a weak band at 1376.3 cm^{-1} appeared on 25 K annealing and increased on further higher temperature annealing. This band is favored in relatively high laser energy experiments, suggesting that more than one metal atom are probably involved. It exhibited no nitrogen-15 shift but was shifted to 992.9 cm^{-1} with ND_3. The isotopic H/D ratio of 1.3861 suggests a Sc−H stretching vibration. This band is tentatively assigned to the $(HSc)_2NH$ molecule. Two weak bands at 1319.3 and 1253.0 cm^{-1} in the Sc + NH_3 reaction produced only on $\lambda > 290$ nm photolysis. These two bands exhibited no nitrogen-15 shift and are most probably due to Sc−H stretching vibrations. These two bands could not be definitively assigned.

Reaction Mechanism

Reactions of early transition metal atoms Sc, Ti, and V with ammonia in solid argon produced the MNH_3 complexes as the primary products. The MNH_3 complex absorptions markedly increased on annealing, indicating that the reactions 1−3 require negligible activation energy.

$$Sc(^2D) + NH_3 \rightarrow ScNH_3(^2E) \qquad \Delta E = -15.4 \text{ kcal/mol} \quad (1)$$

$$Ti(^3F) + NH_3 \rightarrow TiNH_3(^3A_1) \qquad \Delta E = -20.6 \text{ kcal/mol} \quad (2)$$

$$V(^4F) + NH_3 \rightarrow VNH_3(^4E) \qquad \Delta E = -19.7 \text{ kcal/mol} \quad (3)$$

The ^2E ground state of $ScNH_3$ is derived from the $3d^1\ 4s^2$ occupation of Sc, where the unpaired 3d electron is primarily in the $3d_\delta$ (e symmetry) orbital. The Mulliken population analysis shows that the Sc population is $3d^{1.17}4s^{1.83}$. The $^3A_1$ ground state of $TiNH_3$ has an electron configuration of $...(a_1)^2(e)^2$, which correlates mainly with the Ti $3d^24s^2$ ground state. The Ti population is $3d^{2.25}4s^{1.78}$. The VNH_3 was predicted to have a ^4E ground state with $...(a_1)^2(e)^2(e)^1$ configuration, which correlates with the $3d^34s^2$ occupation of V. The V population is $3d^{3.36}4s^{1.69}$. The MNH_3 complexes have also been calculated by Tsipis using an improved modified ASED-MO model; he reported the ground states of $ScNH_3$, $TiNH_3$, and VNH_3 to be ^2E, ^3E, and ^4E, respectively, which are derived from the $3d^34s^0$, $3d^44s^0$, and $3d^54s^0$ occupations of metal atoms.[30] We believe that these states are due to excited states of the complexes.

The experimental observation of stable complexes in the reactions of early transition metals with ammonia is quite different with early transition metal and water reactions.[43−45,48] In the water reactions, metal atoms (Sc, Ti, and V) inserted into the O−H bond of water to form the insertion molecules spontaneously in a solid argon matrix, and no metal−H_2O complex has been experimentally observed. The binding energies of $ScNH_3$, $TiNH_3$, and VNH_3 were estimated to be 15.4, 20.6, and 19.7 kcal/mol, respectively, at the B3LYP/6-311++G-(d,p) level of theory and are larger than those of the corresponding MOH_2 complexes.[45,49,50] As pointed out by Siegbahn et al.,[51] the lone pair orbital of NH_3 is more diffuse than the H_2O lone pairs, and consequently, the dispersion interaction and the σ donation contributed more to the metal−ammonia bond.

The absorptions due to $HScNH_2$, $HTiNH_2$, and $HVNH_2$ appeared on $\lambda > 290$ nm or $\lambda > 400$ nm broadband photolysis, during which the absorptions of complexes disappeared. These observations suggest that the MNH_3 complexes undergo photoinduced isomerization to the $HMNH_2$ molecules, as shown in reactions 4−6. DFT calculations suggest that the inserted $HMNH_2$ molecules are more stable than the MNH_3 complexes.

$$ScNH_3(^2E) \rightarrow HScNH_2(^2A') \qquad \Delta E = -26.7 \text{ kcal/mol} \quad (4)$$

$$TiNH_3(^3A_1) \rightarrow HTiNH_2(^3A'') \qquad \Delta E = -25.4 \text{ kcal/mol} \quad (5)$$

$$VNH_3(^4E) \rightarrow HVNH_2(^4A'') \qquad \Delta E = -21.1 \text{ kcal/mol} \quad (6)$$

The absorptions of $HScNH_2$ decreased on full arc photolysis, during which the ScNH absorption appeared. It implies that near-ultraviolet light initiates H_2 elimination reaction 7 for $HScNH_2$. The ScNH molecules were the dominate product in the reactions of laser-ablated neutral scandium atoms with ammonia in the gas phase.[47] In the Ti and V reactions, no obvious TiNH and VNH absorptions were detected on $\lambda > 290$ nm or even on full arc photolysis. However, the H_2TiNH and H_2VNH molecules were formed on $\lambda > 290$ nm photolysis at the expense of $HTiNH_2$ and $HVNH_2$, suggesting the photoinduced isomerization in reactions 8 and 9.

$$HScNH_2(^2A') \rightarrow ScNH(^2\Sigma^+) + H_2 \qquad \Delta E = 23.8 \text{ kcal/mol} \quad (7)$$

$$HTiNH_2(^3A'') \rightarrow H_2TiNH(^1A') \qquad \Delta E = 7.9 \text{ kcal/mol} \quad (8)$$

$$HVNH_2\ (^4A'') \rightarrow H_2VNH\ (^2A') \qquad \Delta E = 19.5 \text{ kcal/mol} \quad (9)$$

Figures 9−11 show qualitative potential energy surfaces for the Sc, Ti, and V + NH_3 reactions at the B3LYP/6-311++G-(d,p) level. The transition-state structures are shown in Figure 12, and their vibrational frequencies are listed in Table 9. For all three reaction systems, ground-state metal atoms interact with ammonia to form stable complexes. This initial step is barrier free. From the complex, one hydrogen atom transfers from nitrogen to the metal center to form the $HMNH_2$ insertion molecule through a transition state (TS1). This process is exothermic but requires activation energy. The energy barriers were predicted to be 17.4 kcal/mol for Sc, 17.5 kcal/mol for Ti, and 20.9 kcal/mol for V, respectively. As shown in Figure 9, from $HScNH_2$, one hydrogen molecule can be eliminated to form scandium imide ScNH via transition state 2 (TS2). This

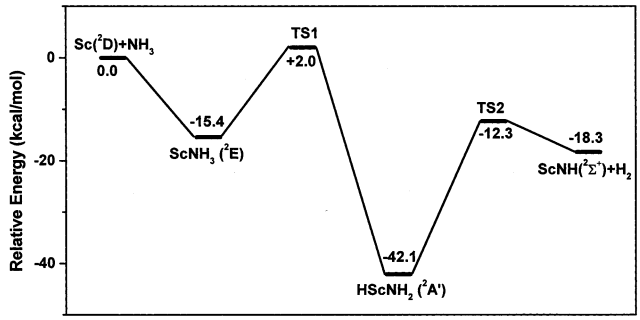

Figure 9. Potential energy surface following the reaction path from $Sc + NH_3$ leading to $ScNH + H_2$ products. Energies given are in kcal/mol and are relative to the ground-state reactants.

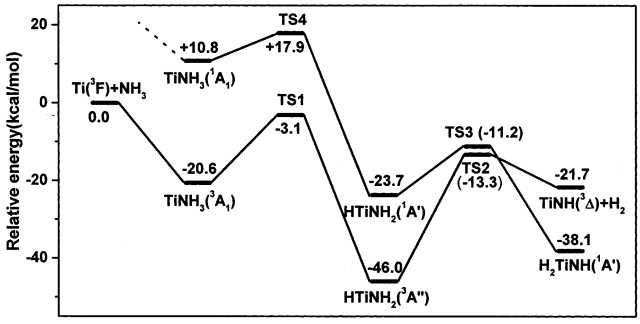

Figure 10. Potential energy surface following the reaction paths from $Ti + NH_3$ leading to the H_2TiNH and $TiNH + H_2$ products. Energies given are in kcal/mol and are relative to the ground-state reactants.

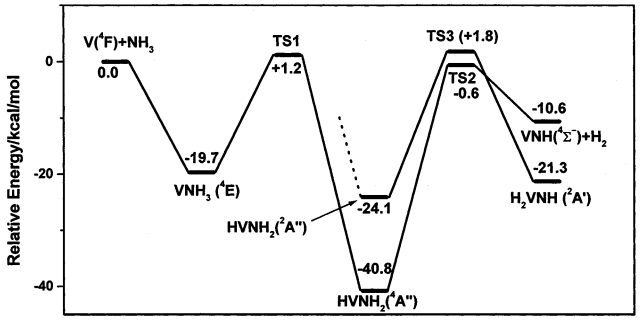

Figure 11. Potential energy surface following the reaction paths from $V + NH_3$ leading to the H_2VNH and $VNH + H_2$ products. Energies given are in kcal/mol and are relative to the ground-state reactants.

process was predicted to be endothermic by about 23.8 kcal/mol with the 29.8 kcal/mol energy barrier. In the Ti and V systems, two paths are possible from $HMNH_2$. One path is the H_2 elimination process to form $MNH + H_2$ analogous to Sc. The other path is the formation of the H_2MNH molecule via spin crossing, as shown in Figures 10 and 11. In both the Ti and V systems, the spin crossing path is energetically favored over the H_2 elimination path. There is no detectable TiNH and VNH produced in the present experiments, and the formation

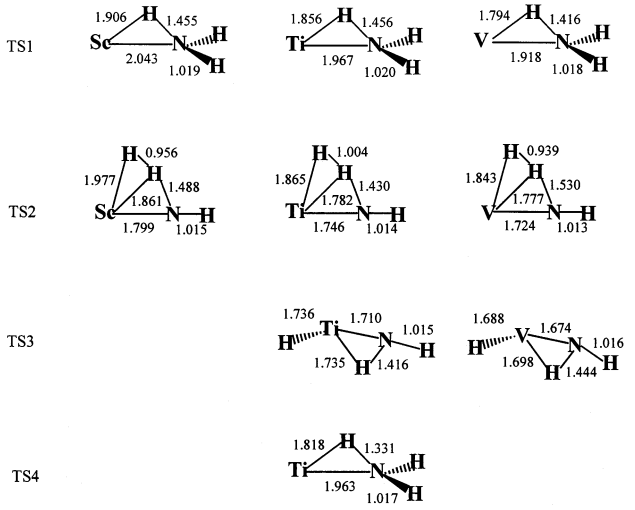

Figure 12. Calculated geometric parameters (bond length in angstrom, bond angle in degree) of the transition states in the potential energy surfaces.

of H_2MNH dominates the reaction, indicating that spin crossing has a very high efficiency in these two reaction systems. The interspin crossing and reactivity in organometallic chemistry has been recently discussed.[52]

It is of particular interest to compare the photochemical reactions of the $HScNH_2$, $HTiNH_2$, and $HVNH_2$ molecules with that of the known $HMNH_2$ molecules (M denotes group 13 and 14 atoms and middle transition metal atoms Mn, Fe, and Ni). The different photochemical behavior of $HMNH_2$ molecules is a direct consequence of the change in valence electron configurations of the M atoms. As Sc has only three valence electrons, there are not enough electrons to satisfy chemical bonding in H_2ScNH, so the H_2 elimination process is the major reaction path of $HScNH_2$. Both titanium and vanadium atoms have enough valence electrons to satisfy the chemical bonding in H_2TiNH and H_2VNH, and the dominant channel is the formation of energetically favored H_2TiNH and H_2VNH. Although middle transition metal atoms have enough valence electrons to satisfy the formation of H_2MNH, this kind of species was not produced by photochemical reactions from $HMNH_2$ (M = Mn, Fe, Ni, etc.) on the basis of exchange energy loss arguments.[53] The $HMnNH_2$ has a $^6A_1$ ground state and the $HFeNH_2$ has a $^5A_2$ ground state.[54] Both molecules have several unpaired metal 3d-based electrons with parallel spin. Apparently, formation of covalently bonded molecules such as H_2MnNH and H_2FeNH will lead to a large loss of exchange energy. For 13 and 14 main group elements, due to the energy separation between valence s and p orbitals, formation of monovalent MNH_2 is energetically favored for group 13 reaction systems, whereas the formation of divalent SiNH is preferred for $HSiNH_2$ reaction.

The oxidative addition of the N−H bond of ammonia to a transition metal center is an important reaction in many catalytic

TABLE 9: Calculated Vibrational Frequencies (cm^{-1}) and Intensities (km/mol) of the Transition States Described in Figure 12

		frequency (intensity)
TS1	Sc	3563.0 (19), 3463.3 (18), 1533.5 (105), 1350.7 (99), 734.1 (97), 723.1 (133), 544.8 (37), 324.5 (13), 1397.1i (1837)
	Ti	3532.9 (26), 3440.8 (8), 1558.3 (79), 1391.1 (96), 825.1 (86), 769.5 (132), 574.9 (26), 451.4 (21), 1368.3i (1311)
	V	3559.8 (30), 3462.4 (24), 1558.9 (70), 1390.1 (70), 863.0 (43), 779.2 (142), 583.6 (40), 454.1 (23), 1405.4i (1537)
TS2	Sc	3572.7 (63), 1920.7 (70), 1769.7 (288), 1165.4 (11), 901.1 (151), 968.5 (39), 724.0 (104), 487.1 (63), 1003.0i (587)
	Ti	3589.6(22,), 3489.4(38), 1546.0 (182), 1449.8 (25), 891.7 (36), 793.0 (187), 566.6 (35), 290.6 (7), 1249.9i (973)
	V	3605.4 (100), 1997.2 (388), 1716.9 (187), 1002.7 (19), 870.8 (241), 838.3 (15), 476.4 (158), 455.2 (135), 989.5i (840)
TS3	Ti	3598.3 (100), 2806.3 (165), 1670.6 (360), 1638.7 (47), 753.5 (147), 589.1 (70), 498.8 (62), 439.5 (48), 39.8i (32)
	V	3555.3 (76), 1757.0 (90), 1712.8 (392), 1060.0 (75), 866.2 (216), 547.6 (129), 472.3 (27), 382.6 (155), 1409.7i (422)
TS4	Ti	3597.2 (96), 1966.0 (39), 1671.5 (183), 1035.5 (11), 936.2 (5), 917.9 (190), 738.0 (125), 393.9 (68), 1232.7i (577)

processes. There are some examples of oxidative addition of ammonia to transition metal complexes. Particularly related to the present study, reactions between ammonia and some early transition metal complexes have been reported. Ammonia reacted with $(Cp_2TiCl)_2$ to yield $Cp_2TiCl(NH_3)$.[55] Bis(titanocene) reacted readily with NH_3 to form a $Cp_4Ti_2N_2H_3$ compound with the evolution of H_2, whereas the zirconium and hafnium complexes $Cp^*_2MH_2$ (M = Zr, Hf) reacted rapidly with ammonia to yield $Cp^*_2M(H)(NH_2)$ and H_2.[56,57] The chemistry of the zerovalent metal atoms reported here exhibits some difference from that of these metals in their high oxidation states.

Conclusions

Reactions of early transition metal atoms Sc, Ti, and V with NH_3 molecules in solid argon matrix have been studied by infrared absorption spectroscopy and density functional theoretical calculations. The metal atoms were produced by pulsed laser ablation of pure metal targets. Various reaction intermediates and products have been identified and characterized by isotopic substitutions and by density functional theoretical frequency calculations.

The ground-state metal atoms (Sc, Ti, and V) reacted with NH_3 to form the MNH_3 (M = Sc, Ti, and V) complexes spontaneously on annealing. These complexes have C_{3v} structure and are correlated with the $3d^n4s^2$ configurations of the metal atoms. Irradiation with near UV or visible light brings about photochemical rearrangement of MNH_3 with insertion of the metal atom into one of the N−H bond of ammonia to form the planar $HMNH_2$ molecules. These photoisomerization reactions are exothermic and proceeded via a transition state. Different photochemical reactions were observed between the $HScNH_2$ molecule and the $HTiNH_2$ and $HVNH_2$ molecules. The $HScNH_2$ molecule decomposed to ScNH upon full arc mercury lamp irradiation. This H_2 elimination process was predicted to be endothermic and requires activation energy. For Ti and V, the novel H_2TiNH and H_2VNH species were generated from the photoinduced isomerization of the $HTiNH_2$ and $HVNH_2$ molecules via spin crossing.

The different photochemical behavior of $HMNH_2$ molecules is a direct consequence of the change in valence electron configurations of the metal atoms. As Sc has only three valence electrons, there are not enough electrons to satisfy chemical bonding in H_2ScNH; the H_2 elimination process is the major reaction path of $HScNH_2$. Both titanium and vanadium atoms have enough valence electrons, and the dominant channel is the formation of energetically favored H_2TiNH and H_2VNH molecule.

The results have also been compared with previous works covering middle transition metal atom as well as main group atom reactions with NH_3, and some periodic trends have been obtained.

Acknowledgment. This work is supported by National Science Foundation of China (Grant Nos. 20003003 and 20125033) and the Chinese NKBRSF.

References and Notes

(1) See, for example: Oyama, S. T. *The Chemistry of Transition Metal Carbides and Nitrides*; Blackie: London, 1996.

(2) See, for examples: Macgregor, S. A. *Organometallics* **2001**, *20*, 1860. Müller, T. E.; Beller, M. *Chem. Rev.* **1998**, *98*, 675. Roundhill, D. M. *Chem. Rev*. **1992**, *92*, 1. Koelliker, R.; Milstein, D. *J. Am. Chem. Soc*. **1991**, *113*, 8524.

(3) Buckner, S. W.; Gord, J. R.; Freiser, B. S. *J. Am. Chem. Soc.* **1988**, *110*, 6606.

(4) Guo, B. C.; Kerns, K. P.; Castleman, A. W., Jr. *J. Phys. Chem.* **1992**, *96*, 4879. MacTaylor, R. S.; Vann, W. D.; Castleman, A. W., Jr. *J. Phys. Chem*. **1996**, *100*, 5329.

(5) Kaya, T.; Kobayashi, M.; Shinohara, H.; Sato, H.*Chem. Phys. Lett*. **1991**, *186*, 431. Sato, H. *Res. Chem. Intermed.* **1993**, *19*, 67.

(6) Clemmer, D. E.; Sunderlin, L. S.; Armentrout, P. B. *J. Phys. Chem.* **1990**, *94*, 208. Clemmer, D. E.; Sunderlin, L. S.; Armentrout, P. B. *J. Phys. Chem*. **1990**, *94*, 3008.

(7) Kooi, S. E.; Castleman, A. W., Jr. *Chem. Phys. Lett*. **1999**, *315*, 49.

(8) Russo, N.; Sicilia, E. *J. Am. Chem. Soc*. **2001**, *123*, 2588.

(9) Ye, S. *THEOCHEM* **1995**, *357*, 147.

(10) Clemmer, D. E.; Armentrout, P. B. *J. Am. Chem. Soc.* **1989**, *111*, 8280.

(11) Hendrickx, M.; Ceulemans, M.; Gong, K.; Vanquickenborne, L. *J. Phys. Chem. A* **1997**, *101*, 8540.

(12) Nakao, Y.; Taketsugu, T.; Hirao, K. *J. Chem. Phys.* **1999**, *110*, 10863.

(13) Marinelli, P. J.; Squires, R. R. *J. Am. Chem. Soc*. **1989**, *111*, 4101.

(14) Walter, D.; Armentrout, P. B. *J. Am. Chem. Soc.* **1998**, *120*, 3176.

(15) Bauschlicher, C. W., Jr.; Langhoff, S. R.; Partridge, H. *J. Chem. Phys.* **1991**, *94*, 2068. Langhoff, S. R.; Bauschlicher, C. W., Jr.; Partridge, H.; Sodupe, M. *J. Phys. Chem.* **1991**, *95*, 10677.

(16) Magnusson, E.; Moriarty, N. W. *Inorg. Chem*. **1996**, *35*, 5711.

(17) Meier, P. F.; Hauge, R. H.; Margrave, J. L. *J. Am. Chem. Soc.* **1978**, *100*, 2108.

(18) Süzer, S.; Andrews, L. *J. Am. Chem. Soc*. **1987**, *109*, 300.

(19) Howard, J. A.; Joly, H. A.; Edwards, P. P.; Singer, R. J.; Logan, D. E. *J. Am. Chem. Soc*. **1992**, *114*, 474.

(20) Lanzisera, D. V.; Andrews, L. *J. Phys. Chem. A* **1997**, *101*, 5082.

(21) Thompson, C. A.; Andrews, L.; Martin, J. M. L.; El-Yazal, J. *J. Phys. Chem.* **1995**, *99*, 13839.

(22) Himmel, H. J.; Downs, A. J.; Greene, T. M. *J. Am. Chem. Soc*. **2000**, *122*, 9793.

(23) Chen, M. H.; Zeng, A. H.; Lu, H.; Zhou, M. F. *J. Phys. Chem. A* **2002**, *106*, 3077.

(24) Kauffman, J. W.; Hauge, R. H.; Margrave, J. L. *High. Temp. Sci*. **1984**, *17*, 237.

(25) Szczepanski, J.; Szczesniak, M.; Vala, M. *Chem. Phys. Lett*. **1989**, *162*, 123.

(26) Ball, D. W.; Hauge, R. H.; Margrave, J. L. *High. Temp. Sci.* **1988**, *25*, 95. Ball, D. W.; Hauge, R. H.; Margrave, J. L. *Inorg. Chem*. **1989**, *28*, 1599.

(27) Bauschlicher, C. W., Jr. *J. Chem. Phys.* **1986**, *84*, 260.

(28) Papai, I. *J. Chem. Phys.* **1995**, *103*, 1850.

(29) Fournier, R. *J. Chem. Phys.* **1995**, *102*, 5396. Chan, W. T.; Fournier, R. *Chem. Phys. Lett.* **1999**, *315*, 257.

(30) Tsipis, A. C. *J. Chem. Soc., Faraday Trans*. **1998**, *94*, 11.

(31) Jackson, K. A.; Knickelbein, M.; Koretsky, G.; Srinivas, S. *Chem. Phys*. **2000**, *262*, 41.

(32) Lacaze-Dufaure, C.; Mineva, T.; Russo, N. *J. Comput. Chem*. **2001**, *22*, 1557.

(33) Blomberg, M. R. A.; Siegbahn, P. E. M.; Svensson, M. *Inorg. Chem.* **1993**, *32*, 4218.

(34) Chen, M. H.; Wang, X. F.; Zhang, L. N.; Yu, M.; Qin, Q. Z. *Chem. Phys*. **1999**, *242*, 81.

(35) Frisch, M. J.; Trucks, G. W.; Schlegel, H. B.; Scuseria, G. E.; Robb, M. A.; Cheeseman, J. R.; Zakrzewski, V. G.; Montgomery, J. A., Jr.; Stratmann, R. E.; Burant, J. C.; Dapprich, S.; Millam, J. M.; Daniels, A. D.; Kudin, K. N.; Strain, M. C.; Farkas, O.; Tomasi, J.; Barone, V.; Cossi, M.; Cammi, R.; Mennucci, B.; Pomelli, C.; Adamo, C.; Clifford, S.; Ochterski, J.; Petersson, G. A.; Ayala, P. Y.; Cui, Q.; Morokuma, K.; Malick, D. K.; Rabuck, A. D.; Raghavachari, K.; Foresman, J. B.; Cioslowski, J.; Ortiz, J. V.; Stefanov, B. B.; Liu, G.; Liashenko, A.; Piskorz, P.; Komaromi, I.; Gomperts, R.; Martin, R. L.; Fox, D. J.; Keith, T.; Al-Laham, M. A.; Peng, C. Y.; Nanayakkara, A.; Gonzalez, C.; Challacombe, M.; Gill, P. M. W.; Johnson, B. G.; Chen, W.; Wong, M. W.; Andres, J. L.; Head-Gordon, M.; Replogle, E. S.; Pople, J. A. *Gaussian 98*, revision A.7; Gaussian, Inc.: Pittsburgh, PA, 1998.

(36) Becke, A. D. *J. Chem. Phys.* **1993**, *98*, 5648.

(37) Lee, C.; Yang, E.; Parr, R. G. *Phys. Rev. B* **1988**, *37*, 785.

(38) See for examples: Bauschlicher, C. W., Jr.; Ricca, A.; Partridge, H.; Langhoff, S. R. In *Recent Advances in Density Functional Theory*; Chong, D. P., Ed.; World Scientific Publishing: Singapore, 1997; Part II. Bauschlicher, C. W., Jr.; Maitre, P. *J. Chem. Phys.* **1995**, *99*, 3444. Bytheway, I.; Wong, M. W. *Chem. Phys. Lett*. **1998**, *282*, 219. Siegbahn, P. E. M. Electronic Structure Calculations for Molecules Containing Transition Metals. *Adv. Chem. Phys*. **1996**, XCIII. Hartmann, M.; Clark,

T.; Van Eldik, R. *J. Am. Chem. Soc.* **1997**, *119*, 7843. Irigoras, A.; Fowler, J. E.; Ugalde, J. M. *J. Am. Chem. Soc.* **1999**, *121*, 574.

(39) McLean, A. D.; Chandler, G. S. *J. Chem. Phys.* **1980**, *72*, 5639. Krishnan, R.; Binkley, J. S.; Seeger, R.; Pople, J. A. *J. Chem. Phys.* **1980**, *72*, 650.

(40) Wachter, J. H. *J. Chem. Phys.* **1970**, *52*, 1033. Hay, P. J. *J. Chem. Phys.* **1977**, *66*, 4377.

(41) Head-Gordon, M.; Pople, J. A.; Frisch, M. *Chem. Phys. Lett.* **1988**, *153*, 503.

(42) Suzer, S.; Andrews, L. *J. Chem. Phys.* **1987**, *87*, 5131.

(43) Kauffman, J. W.; Hauge, R. H.; Margrave, J. L. *J. Phys. Chem.* **1985**, *89*, 3547.

(44) Zhang, L. N.; Dong, J.; Zhou, M. F. *J. Phys. Chem. A* **2000**, *104*, 8882.

(45) Zhou, M. F.; Zhang, L. N.; Dong, J.; Qin, Q. Z. *J. Am. Chem. Soc.* **2000**, *122*, 10680.

(46) *CRC Handbook*; CRC Press: Boca Raton, FL, 1985. (^{46}Ti, 8.0%; ^{47}Ti, 7.5%; ^{48}Ti, 73.7%; ^{49}Ti, 5.5%; ^{50}Ti, 5.3%)

(47) Steimle, T. C.; Xin, J.; Marr, A. J.; Beaton, S. *J. Chem. Phys.* **1997**, *106*, 9084.

(48) Zhou, M. F.; Dong, J.; Zhang, L. N.; Qin, Q. Z. *J. Am. Chem. Soc.* **2001**, *123*, 135.

(49) Zhang, L. N.; Shao, L. M.; Zhou, M. F. *Chem. Phys.* **2001**, *272*, 27.

(50) Guo, J. Z.; Goodings, J. M. *Chem. Phys. Lett.* **2001**, *342*, 169. Hwang, D. Y.; Mebel, A. M. *Chem. Phys. Lett.* **2001**, *341*, 393.

(51) Siegbahn, P. E. M.; Blomberg, M. R. A.; Svensson, M. *J. Phys. Chem.* **1993**, *97*, 2564.

(52) Schroder, D.; Shaik, S.; Schwarz, H. *Acc. Chem. Res.* **2000**, *33*, 139, and references therein. Plattner, D. A. *Angew. Chem., Int. Ed. Engl.* **1999**, *38*, 82.

(53) Carter, E. A.; Goodard, W. A., III *J. Am. Chem. Soc.* **1986**, *108*, 2180. Carter, E. A.; Goodard, W. A., III *J. Phys. Chem.* **1988**, *92*, 5679.

(54) Shao, L. M.; Zhou, M. F. Manuscript to be published.

(55) Green, M. L. H.; Lucas, C. R. *J. Chem. Soc., Dalton Trans.* **1972**, 1000.

(56) Casalnuovo, A. L.; Calabrese, J. C.; Milstein, D. *Inorg. Chem.* **1987**, *26*, 971;

(57) Hillhouse, G. L.; Bercaw, J. E. *J. Am. Chem. Soc.* **1984**, *106*, 5472.